INTERNATIONAL JOURNAL OF Electroactive Materials

Int. J. Electroactive Mater. **6 (2018) 1-7**
www.electroactmater.com

RECEIVED
06 January 2018

REVISED
15 March 2018

ACCEPTED FOR PUBLICATION
17 March 2018

PUBLISHED
28 March 2018

Dye-sensitized solar cell utilizing TiO_2-NiS composite photoanode: Effect of nickel nitrate concentration on its performance

S.N. Sadikin, M.Y.A. Rahman*, A.A. Umar

Institute of Microengineering and Nanoelectronics (IMEN), Universiti Kebangsaan Malaysia, 43600, Bangi, Selangor, Malaysia
E-mail: mohd.yusri@ukm.edu.my *

ABSTRACT: TiO_2-NiS composite films prepared via sol-gel method assisted spin-coating technique has been utilized as photoanode of dye-sensitized solar cell (DSSC). The concentration of the nickel nitrate precursor was varied. The influence of the concentration of the precursor on the structural, optical properties and photovoltaic performance has been investigated. The XRD studies revealed that the samples are crystalline with the presence of NiS and anatase TiO_2 phase. The samples absorb more light in ultraviolet region. The highest efficiency of 0.137% was achieved at 3 mM nickel nitrate due to the smallest crystallite size and lowest charge transfer resistance at TiO_2-NiS/dye/electrolyte interface.
Keywords: composite, dye-sensitized solar cell, nickel sulfide, photoanode

1. Introduction

Improving the power conversion efficiency of dye-sensitized solar cell (DSSC) can be achieved in many ways such as employing various metal oxide semiconductors as photoanode, modifying the surface structure of the photoanode and introducing new materials into the commonly used metal oxide semiconductor for photoanode. For example, Hu et al. studied the doping of Ag in TiO_2 nanotube arrays and used it as the photoanode for DSSC [1]. As a result, the power conversion efficiency was improved significantly from 3.00% to 6.12%. The doping of Ag causes the formation of cluster structure and contributes to larger surface area.

Zhu et al. studied the photoelectrochemical properties of DSSC utilizing graphene-TiO_2 composite photoanodes [2]. He discovered that the integration of graphene nanosheets in TiO_2 contributes to higher capability of photogenerated electron transfer as well as reduced the charge recombination of electron and hole. Another study by Rao et al. shows the increment in the power conversion efficiency of DSSC utilizing ZnS coated TiO_2 photoanode [3]. The efficiency increased from 4.43% to 5.90%. Introducing ZnS as the blocking layer inhibits the rate of electrons and holes recombination at the interface between TiO_2-electrolyte. Pham et al. reported that light trapping efficiency of the device was enhanced by modifying the morphology of TiO_2 [4]. A mesoporous-macroporous nanostructure was invented in order to improve the efficiency of photogenerated electron due to the scattering effect in the structure. This approach resulted in enhancement of power conversion efficiency.

In this work, TiO_2-NiS composite synthesized via sol-gel method was utilized as photoanode of DSSC. The originality of this work is the use of the composite as photoanode of the device. The concentration of nickel nitrate precursor was varied and the effect of $Ni(NO_3)_2$ concentration on the properties of TiO_2 films and the performance of DSSC was investigated.

2. Experimental

2.1 Preparation and characterization of TiO_2-NiS films

Pure TiO_2 solution without NiS was firstly synthesized by using sol-gel method in which 1.05 ml of titanium (IV) butoxide (97.0%, purchased from Sigma Aldrich) is added into 8.78 ml of ethanol dropwise and under stirring at high rpm. Then, 0.17 ml of acetic acid (99.7%, purchased from Sigma Aldrich) and triton x was added into the solution at the final step. The solution was left under high stirring for about 5 hours at room temperature.

TiO_2-NiS solution was prepared by dissolving nickel nitrate and thiourea in ethanol with the molar ratio of 1:2. Then, titanium (IV) butoxide was added drop by drop into the solution. Acetic acid and triton were then added into the solution. The solution was left under stirring at high rpm for 5 hours at room temperature. Four different concentrations of nickel nitrate and thiourea in TiO_2 were prepared. The samples were prepared by depositing the solution on ITO substrates by using spin-coating method. In this method, TiO_2-NiS solution was dropped on clean ITO substrates and rotated at 800 rpm for about 30 seconds. The samples were then heated at 100 ^oC for 15 minutes on a hot plate to let the deposition on the substrates to dry out. The processes were repeated for 5 times to obtain good thin films. Finally, the prepared TiO_2-NiS thin films were annealed at 450 ^oC for 3 hours.

To study the phase and crystallinity of the samples, XRD characterization was carried out by using x-ray diffractometer model Bruker D8 Advanced at diffraction angles of 10º to 80º. The optical property of the samples was also studied by using the UV-Vis spectrophotometer.

2.2 Dye-sensitized solar cell (DSSC) fabrication and characterization

The performance of the DSSC utilizing TiO_2-NiS samples in DSSC was studied by using Gamry instrument. The device was fabricated by utilizing the TiO_2-NiS film sensitized with N719 dye as the photoanode and platinum film as counter electrode. The device fabrication has been described in our previous work [5]. The electrolyte of iodolyte containing iodide/triiodide redox couple was then injected into the active area between TiO_2-NiS-N719 and platinum counter electrode. The current-voltage characteristics were obtained in the dark and under light illumination of 100 mW cm^{-2}. The electrochemical impedance spectroscopy (EIS) measurement was also carried out to study the charge transport properties in the device.

3. Results and discussion

Fig. 1 shows the XRD spectra for TiO_2-NiS films with different concentrations of NiS. The XRD analysis shows that the TiO_2 is mainly in anatase phase. It can be proven from the peaks shown in **Fig. 1**. There are 5 distinct peaks at the diffraction angles and planes as follows, 25.64º (101), 38.24º (004), 48.46º (200), 55.56º (211) and 63.22º (213). The intensity of TiO_2 peak at 25.64º is observed to decrease as the concentration of NiS increases. For the samples containing NiS, there are two distinct peaks for NiS which are at the diffraction angles and planes of 48.50º (111) and 56.0º (056). The NiS phase is observed to present in all samples. The average crystallite size for all samples were determined from Scherrer formula and presented in **Table 1**. From the table, it is noticeable that the crystallite size does not change significantly with the concentration of nickel nitrate. It can be concluded that the concentration does not influence the crystallite size of the sample.

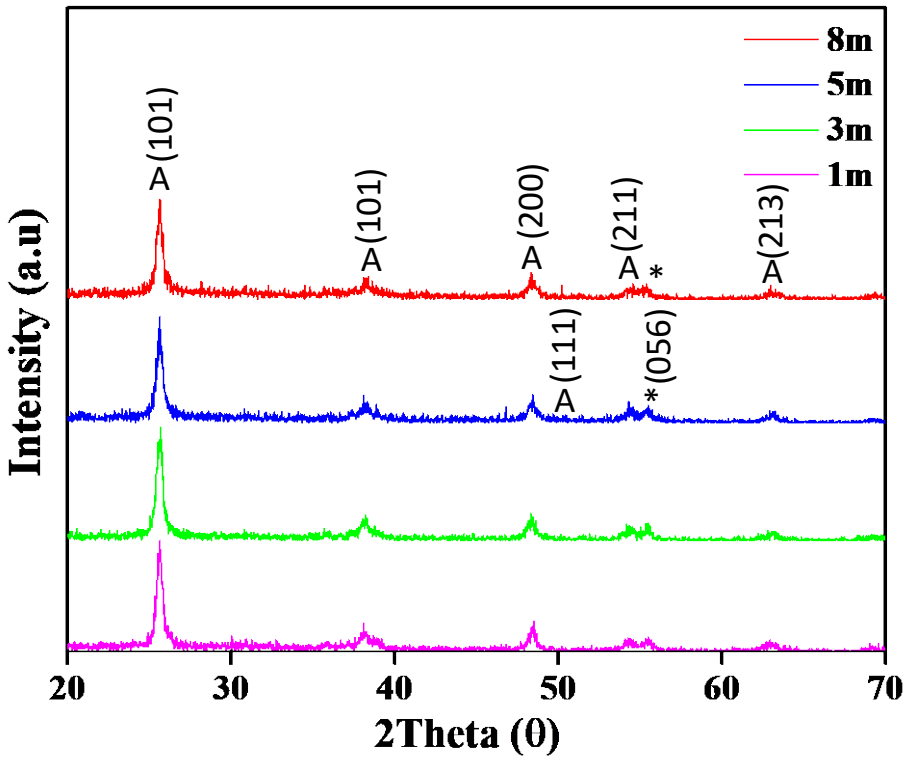

Figure 1: XRD spectra for TiO_2-NiS films with different concentrations of nickel nitrate. A - Anatase and * - NiS

Table 1: Average crystallite size for the samples with various nickel nitrate concentrations

Concentration (mM)	Average crystallite size (nm)
1	22.1
3	20.7
5	23.8
8	21.3

Fig. 2 shows the optical absorption spectra of TiO_2-NiS samples with different concentration of NiS. The TiO_2 sample prepared with 3 mM nickel nitrate precursor shows the highest light absorption in the visible light region. The sample of TiO_2-NiS with 8 mM nickel nitrate concentration shows the lowest absorption in the visible region. This indicates that higher concentration of NiS in the sample reduces the ability of the sample to absorb more light. The introduction of NiS in the TiO_2 promotes the faster electron transfer since NiS has a positive photoconductivity [6]. However, as the content of NiS increases, the overload of NiS particles on TiO_2 surface might hinder the TiO_2 particles from absorbing light. This decreases the optical absorption of the sample and thus reduces the power conversion efficiency of the device as illustrated in Table 2. Also from the figure, all samples shows lower absorption in visible region (400-700 nm) compared with UV region (300-400 nm).

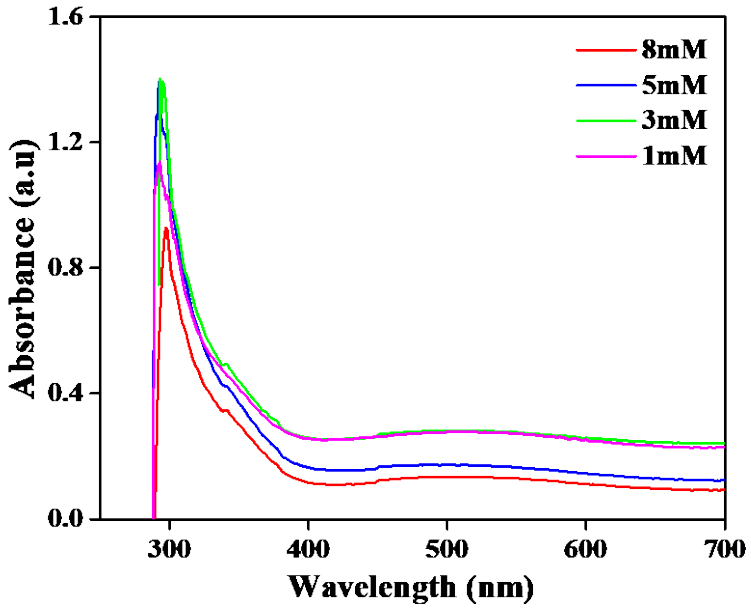

Figure 2: UV-Vis absorption spectra for TiO_2-NiS films with various concentrations of nickel nitrate

Fig. 3 illustrates the dark current curves of all devices with various concentrations of nickel nitrate. It is noticeable that the dark current in reverse bias is slightly higher than that in forward bias for all devices. This means that the leak current is slightly higher than the forward bias current causing more power loss in the device and consequently lowers the power conversion efficiency as illustrated in **Table 2**. Higher leak current means higher recombination rate of electron-hole. It is also observed that the dark current is not affected by the concentration of nickel nitrate.

The *J-V* curves under illumination of the device utilizing TiO_2-NiS photoanode with various nickel nitrate concentrations are shown in **Fig. 4**. The slope of the curve with 3 mM sample is high, resulting in high power loss. The tangent slope near the V_{oc} associates with the series resistance which represents the internal resistance of the charge transfer at the electrolyte/platinum electrode [7]. High series resistance might due to the shorter time between the electrolyte injection and the testing of device. The longer time between the two processes enhances the amount of electrolyte contact with the dye-adsorbed TiO_2 [8]. Lower amount of electrolyte in contact with the dye-adsorbed TiO_2 reduces the charge transfer rate between dye and electrolyte, resulting in higher resistance. The other three devices possess low output power indicated by the small area under curves. The device utilizing 3 mM sample has the highest output power, followed by the sample with 1, 5 and 8 m in descending order. The photovoltaic parameters are extracted from the figure and illustrated in **Table 2**.

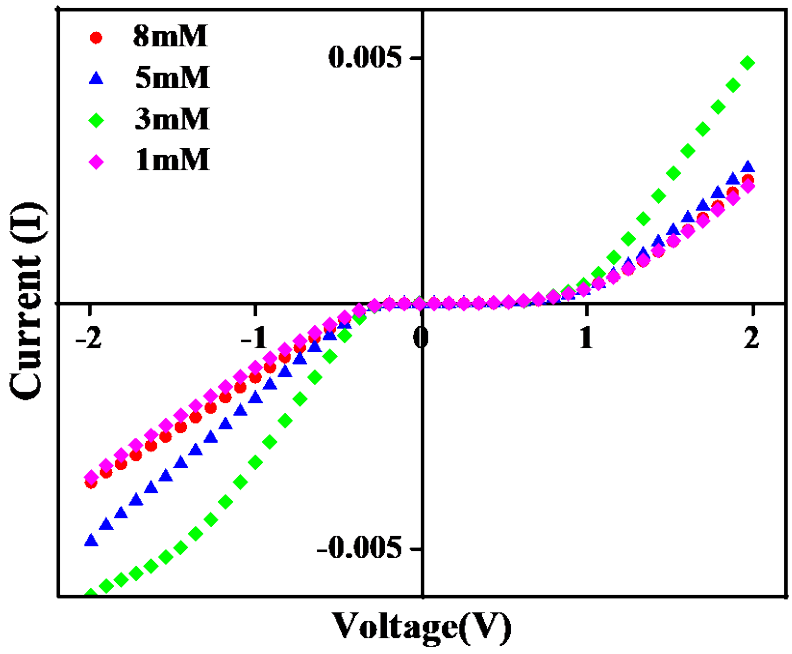

Figure 3: Dark current of DSSC with different concentrations of nickel nitrate precursor

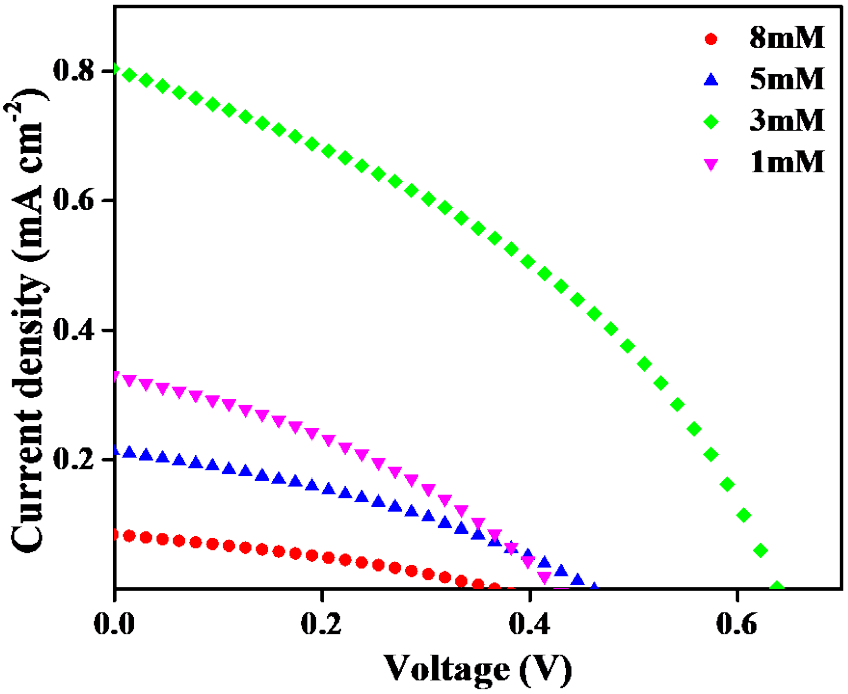

Figure 4: *J-V* curves of DSSC with different concentrations of nickel nitrate precursor under 100 mWcm^{-2} light illumination

From **Table 2**, it is noticed that the highest photovoltaic parameters are obtained for 3 mM sample. The device utilizing 8 mM sample demonstrates the lowest photovoltaic parameters. There is no increasing or decreasing trend of photovoltaic parameters with the concentration of $Ni(NO_3)_2$. The increase of power conversion efficiency can be related with the crystallite size of the sample. The highest efficiency of 0.137% is obtained by the device with 3 mM sample. According to Table 1, this sample has the smallest crystallite size resulting in the highest area for dye loading. From this observation, it can be deduced that smaller crystallite size gives larger specific surface area as studied by Gaber et al. [9]. Thus, it provides larger area for dye adsorption, improving the absorption in the visible light region [10]. When more light is trapped, it aids the transport of electron and enhance the power conversion efficiency [11]. From **Fig. 2**, it is observed that the 3 and 8 mM sample possess the highest and lowest optical absorption, respectively. The efficiency become lower when the concentration is further increased. This is because the optical absorption decreases when the concentration is further increased to 5 and 8 mM. This degrades dye adsorption and consequently reduces the lower effective density of states for TiO_2 conduction band and in turn yields lower efficiency as reported by Dou et al. [12]. While, the fill factor is low for all devices since the slope of the *J-V* curves is high as shown in **Fig. 4**.

Fig. 5 depicts the Nyquist plots of the device with various concentration of nickel nitrate. The impedance spectra show three semi-circles for which the smallest semi-circle represents the bulk resistance (R_b), the middle semicircle denotes the charge transfer resistance at the interface of TiO_2-NiS/dye/electrolyte (R_{ct1}) and the biggest one indicates the charge transfer resistance at the electrolyte/platinum electrode interface (R_{ct2}). However, the impedance spectrum for the device with 5 mM nickel nitrate concentration has four semi-circles. This might due to the existence of unidentified phase other than NiS or TiO_2 in the photoanode that contributes to another interface boundary in the device. All resistances are determined from the real impedance (Z) and illustrated in **Table 3**. These EIS data can also be used to explain the photovoltaic parameters listed in the table. From the table, the device utilizing 3 mM sample has the lowest R_{ct1}, yielding the highest efficiency. The device with 8 mM sample demonstrates the lowest efficiency which is due to the lowest $R_{ct1.}$ The change in R_{ct1} with concentration of nickel nitrate precursor might be due to the change of the crystallite size of TiO_2-NiS composite. According to **Table 1** and 3, the R_{ct1} increases with the crystallite size of the composite.

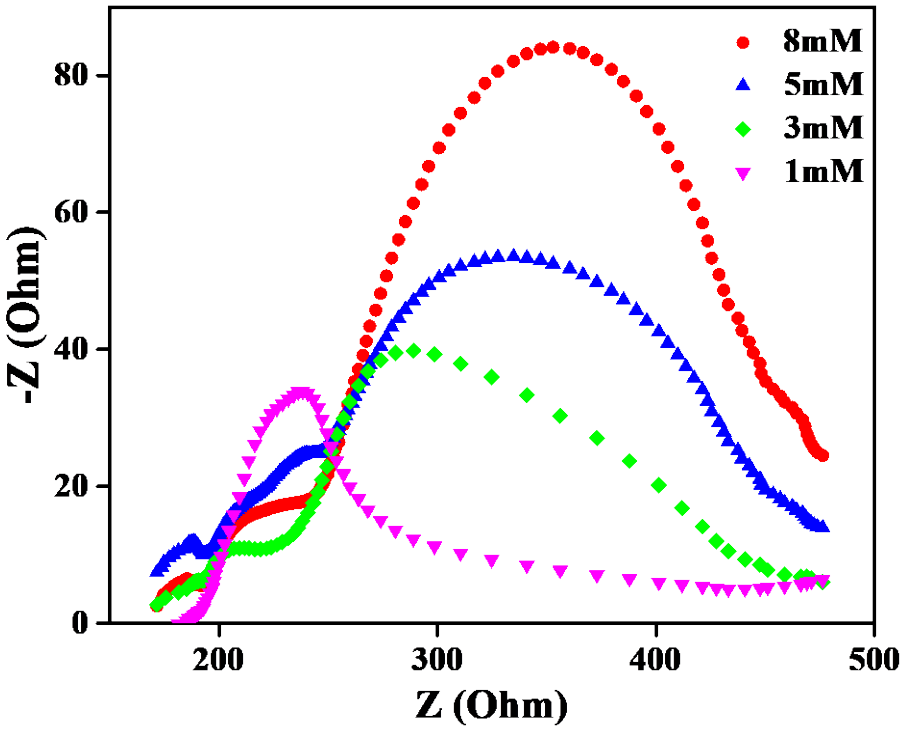

Figure 5: Nyquist plots with different concentrations of nickel nitrate precursor under 100 mW cm^{-2} light illumination

Table 2: Photovoltaic parameters for DSSC with different concentrations of nickel nitrate precursor

Concentration (mM)	J_{sc} (mA cm^{-2})	V_{oc} (V)	η (%)	*FF*
1	0.323 ± 0.003	0.441± 0.013	0.048 ± 0.001	0.341 ± 0.011
3	0.581 ± 0.114	0.603 ± 0.018	0.137 ± 0.033	0.385 ± 0.004
5	0.152 ± 0.033	0.386 ± 0.045	0.021 ± 0.007	0.330 ± 0.009
8	0.074 ± 0.006	0.334 ± 0.018	0.008 ± 0.001	0.319 ± 0.003

Table 3: EIS parameters for DSSC with various concentrations of nickel nitrate precursor

Concentration (mM)	R_b (Ω)	R_{ct1} (Ω)	R_{ct2} (Ω)
1	54	104	143
3	54	95	158
5	57	101	122
8	57	132	141

4. Conclusions

TiO_2-NiS composite film has been prepared and applied as a photoanode in dye-sensitized solar cell. The device applying the 3 mM sample demonstrates the highest power conversion efficiency of 0.137%. This is due to this device utilizing the sample with the lowest crystallite size and highest optical absorption. Furthermore, this device possesses the lowest charge interfacial resistance at the interface TiO_2-NiS/dye/electrolyte.

Acknowledgement

The authors would like to thank UKM for providing financial support to this work via a research grant GUP-2016-013.

References

1. J. Hu, J. Cheng, S. Tong, Y. Yang, M. Cheng, S. Hu, Int. J. Photoenergy 2736257 (2016) 9 pages.
2. M. Zhu, X. Li, W. Liu, Y. Cui, J. Power Sources 262 (2014) 349-355.
3. S. Srinivasa Rao, D. Punnoose , Ch. Venkata Tulasivarma, C.H. Pavan Kumar, C.V. Gopi, S.K. Kim, H.J. Kim, Dalt. Trans. 44 (2015) 2447-2455.
4. T.T. T. Pham, N. Mathews, Y.-M. Lam, S. Mhaisalkar, J. Electron. Mater. 46 (2017) 3801-3807.
5. S.N. Sadikin, M. Y. A. Rahman, A. A. Umar, M. M. Salleh, Int. J. Electrochem. Sci. 12 (2017) 5529–5538.
6. S. Suresh, S.S.R. Solay Anand, R. Arul, D. Isha, Chalcogenide Letters. 13 (2016) 291-299.
7. A. McEvoy, T. Markvart, L. Castaner. (2013) Solar Cells: Materials, Manufacture and Operation, Second Edition. Oxford, UK: Elsevier.
8. R.Y. Yang, H.Y. Chen, F.D. Lai, Adv. Mater. Sci. & Eng. 2012 (2012) 4 pages.
9. A. Gaber, M.A. Abdel-Rahim, A. Y. Abdel-Latief, M. N. Abdel-Salam, ,Int. J. Electrochem. Sci. 9 (2014) 9 81-95.
10. J. Zhang, W. Peng, Z. Chen, H. Chen, L. Han, J. Phys. Chem. C 116 (2012) 19182-19190.
11. Q. Hu, C. Wu, L. Cao, B. Chi, J. Pu, L. Jian, J. Power Sources 226 (2013) 8-15.
12. Y. Dou, F.Wu, G. Liu, C. Mao, K. Wan,, M. Zhou, J. Power Sources 307 (2016) 181-189.